ATMOSPHERIC CO_2 DEPLETION NEAR THE SURFACE IN THE MARTIAN POLAR REGIONS

S. Piqueux, *Jet Propulsion Laboratory, California Institute of Technology, Pasadena, USA (sylvain.piqueux@jpl.caltech.edu)*, **P.O. Hayne**, *Department of Astrophysical and Planetary Sciences and Laboratory for Atmospheric and Space Physics, University of Colorado Boulder, Boulder, CO, USA,* **A. Kleinböhl, D.M. Kass, M. Schreier**, *Jet Propulsion Laboratory, California Institute of Technology, Pasadena, USA*, **D.J. McCleese, J.T. Schofield,** *Jet Propulsion Laboratory, Retired,* **J.H. Shirley**, *Jet Propulsion Laboratory, Retired, now TORQUEFX LLC,* **N. Heavens**, *Space Science Institute, Boulder, CO, USA,* **M.I. Richardson**, *Aeolis Research, Chandler, AZ, USA.*

Introduction: The yearly waxing and waning of the seasonal polar caps represents one of the most dramatic expressions of the CO_2 cycle on Mars, with massive amounts of carbon dioxide cyclically exchanged between the atmosphere and the surface [1]. As CO_2 condenses on the surface, non-condensable (*NC*) species (Ar, N_2, CO, etc.) are left behind and accumulate in the atmosphere, resulting in a decrease of the CO_2 partial pressure P_{CO2} and thus a reduction of the CO_2 frost point temperature T_{CO2} [2].
Throughout the exploration of Mars, infrared brightness temperatures of the seasonal caps as low as ~ 13 K below T_{CO2} have been observed. These "cold spots" were attributed, at least in part, to enrichment in non-condensable gases [2-5], although clouds [3,6], snowfall [3,7], and small low emissivity ice crystals on the ground [8-11] have also been implicated. Nonetheless, the observed seasonal enrichment in *NC* by factors as large as ~ 6 in the atmospheric column, at least in the South [12-14] has confirmed that the reduction of surface temperatures may have an impact on the polar energy budget and global climate [15].

We contribute to this characterization of the Mars near-surface atmosphere and present an analysis of Mars Climate Sounder (MCS [16], onboard Mars Reconnaissance Orbiter) thermal infrared observations of the Martian seasonal cap and estimate the near-surface mixing ratio for CO_2 and non-condensable gases as a function of season and latitude. We discuss these results in terms of regional near-surface atmospheric circulation patterns, and speculate on the implications for energy balance and near-surface regolith properties at polar and high latitudes.

Approach: We use MCS atmospherically-corrected brightness temperature observations of the seasonal caps centered at two wavelengths $\lambda \sim 12$ μm (T_{12}) and $\lambda \sim 22$ μm (T_{22}) to determine the kinetic temperature of the cap T_{CO2} and the associated equilibrium CO_2 gas pressure P_{CO2} using [17]. We compare this partial pressure P_{CO2} with a climatological prediction of the local atmospheric pressure P taken from the EMARS assimilation database [30] to derive the local CO_2 mixing ratio MR_{CO2} at the surface of the seasonal caps.

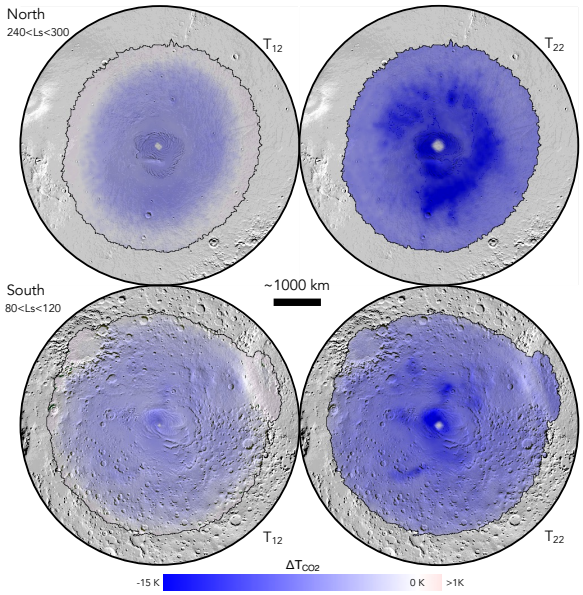

Figure 1: *ΔT_{CO2}, the difference between 1) T_{12} (T_{22}) brightness surface temperatures of the North at 240 < L_s < 300° (South, at 80° < L_s < 120 °) and 2) the climatological frost point determined using surface pressures P[18,19]. Each panel covers the pole down to 40° in latitude. Grey background is a MOLA [20] shaded relief map. Maximum extent of the cap is shown as black contours from [21].*

Deriving T_{CO2}. MCS-retrieved surface temperatures convolve two unknowns: the kinetic temperature of the ice T_{CO2} (the quantity necessary to derive P_{CO2}), and the CO_2 ice emissivity, strongly wavelength-dependent and itself controlled by CO_2 crystal sizes [22-25]. *Fig. 1* provides a concrete illustration of this differential behavior for T_{22} and T_{12} (or ΔT_{CO2}, expressing the difference between T_{22} or T_{12} and T_{CO2}) after normalization with respect to the local theoretical frost point (to eliminate topographic effects). While T_{22} shows recognizable ground patterns of low surface emissivity features at discreet locations that are interpreted as snow deposits [26,7], the T_{12} maps are generally featureless, warmer, and display a trend of lower temperatures towards the poles. The kinetic temperature of the ice T_{CO2} cannot directly be inferred from these maps.

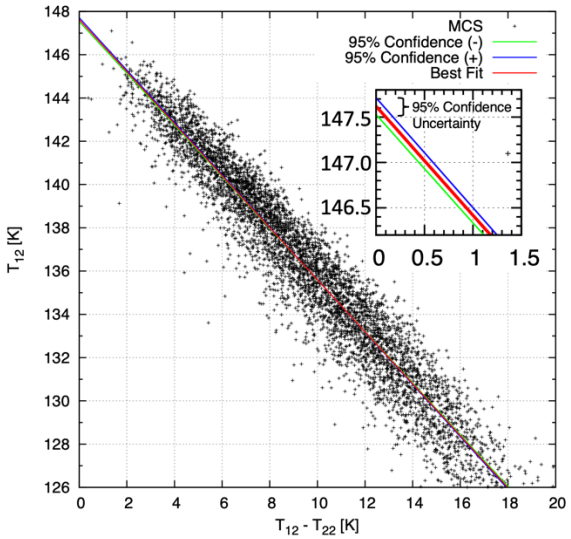

Figure 2: *Example of a linear fit between T_{12} and T_{22}, near the north pole (80-90°N) using data acquired at 240° < L_s < 250°. Best fit yields T_{CO2} = 147.7 K, with 95% confidence between 147.6 and 147.8 K.*

Nonetheless, a fortuitous pseudo-linear relationship between the CO_2 ice brightness temperatures T_{12} and T_{22} was first identified by [27], who showed that a linear regression through a collection of observations yields the surface temperature where the surface emissivity ~1. (i.e., where T_{12} and $T_{22} = T_{CO2}$) at the intercept. [3] (their Fig. 6) first leveraged this linear relationship to derive CO_2 partial pressures for the purpose of estimating depletion.

Leveraging this linearity, MCS T_{12} and T_{22} observations are binned latitudinally (10°) and seasonally (in steps of 10° of L_s) to derive the local kinetic temperature of the ice T_{CO2} through a set of temporal and spatial fits (Fig. 2). This approach requires the following assumptions to be true:

1. T_{CO2} must be uniform within a spatial bin, because a single best-fit T_{CO2} value is derived from a set of observations falling within a bin. To limit T_{CO2} variability, the spatial binning is defined by 10° latitude bands as topography, atmosphere circulation, and depletion are generally axisymmetric and centered on the poles [6];
2. Seasonal variability must be small within 10° of L_s compared to the time scale of changes in depletion reported in the literature [13,14];
3. A spatial bin must contain diverse CO_2 crystal sizes to observe a significant spread of T_{12} and T_{22} values, otherwise a linear fit through the data would be meaningless. Because cold spots are spatially widespread [26,3,7,11,25], the majority of the bins display a wide range of brightness temperatures and meet this requirement.

Contamination by dust and water prevents an accurate derivation of the surface crystal sizes, yielding nearly unit emissivity surfaces, but this limitation does not impact the linear relationship between T_{22} and T_{12} - T_{22} or our ability to derive the kinetic temperature of the ice. In each spatial and temporal bin, three fits are performed (*Fig. 2*): the best fit, whose intercept provides T_{CO2}, and two regressions whose intercept yield the upper and lower 95% confidence values. When errors bars are reported, they correspond to the 95% confidence intervals (see *Fig. 3*). [6] present a comparable approach using observations at 11 and 20 µm by the InfraRed Thermal Mapper [28] in conjunction with a model of CO_2 ice emissivity to derive T_{CO2}.

Mixing Ratios and Enhancement Factors. CO_2 mixing ratios MR_{CO2} are calculated as follow:

$$MR_{CO2} = P_{CO2} / P \quad (1)$$

with P the atmospheric pressure on the ground when no depletion is taking place [18]; for non-condensable gases (MR_{NC}):

$$MR_{NC} = 1. - MR_{CO2} \quad (2)$$

The non-condensable gas enrichment factor EF_{NC} is calculated as follows:

$$EF_{NC} = MR_{NC} / (1. - \underline{MR_{CO2}}) \quad (3)$$

with $\underline{MR_{CO2}} = 0.957$ [29]. Fig. 3 displays the binned non-condensable enhancement factor EF_{NC} (chosen to facilitate a comparison with the Gamma Ray Spectrometer results [30]) vs. latitude and Ls.

Results and Discussion: In both hemispheres, the depression peaks of the caps kinetic temperature are ~ 2.9-3.8 K in the South and ~ 3.7-4.0 K for the North, which is lower than the ~ 5 K reported by [6]. While [6] find kinetic temperature decreasing towards both poles, our analysis does not show this latitudinal trend in the North. In addition, seasonal trends are now identified (*Fig. 3*). Using Eq. 1-4, we derive EF_{NC} from the ice temperature.

In the North, EF_{NC} (*Fig. 3*) approximately follows a seasonal and latitudinal trend aligned with the growth and retreat of the caps: peak enrichment is maximum in the 90°-80°N near Ls ~ 215° (EF_{NC} = 8.7), followed by progressively lesser values occurring at later seasons for terrains closer to the edges of the caps (i.e., EF_{NC} = 8.5 at Ls ~ 235° in 80°-70°N, EF_{NC} = 8.3 at Ls ~ 245° in 70°-60°N, EF_{NC} = 8.0 at Ls ~ 265° in 60°-50°N). When the cap is growing the fastest near L_s ~ 290° [31], most terrains display relatively similar depletion values (i.e., EF_{NC} ~ 7-8). The solstitial pause [32,33] characterized by a weakening of the polar vortex between L_s ~ 240° and L_s ~ 290° is associated with a modest seasonal minimum of the enrichment between 90ºN and 70ºN, even though the cap is still condensing. Near L_s = 330°, the mass of CO_2 on the ground is reaching its peak and the depletion mechanism is shutting off, followed by massive re-injection of CO_2 from the ground, which results in a rapid decrease of EF_{NC}.

The 90°-60°N bands tend to display similar trends, but data in the 60°-50°N band stand out, with large oscillations super-imposed on the general trend reported above. Such large oscillations are not observed in the South, within any of the latitude bands.

We note that the terrains closest to the geographic pole (i.e., 90°-80°N) do not display the lowest sur-

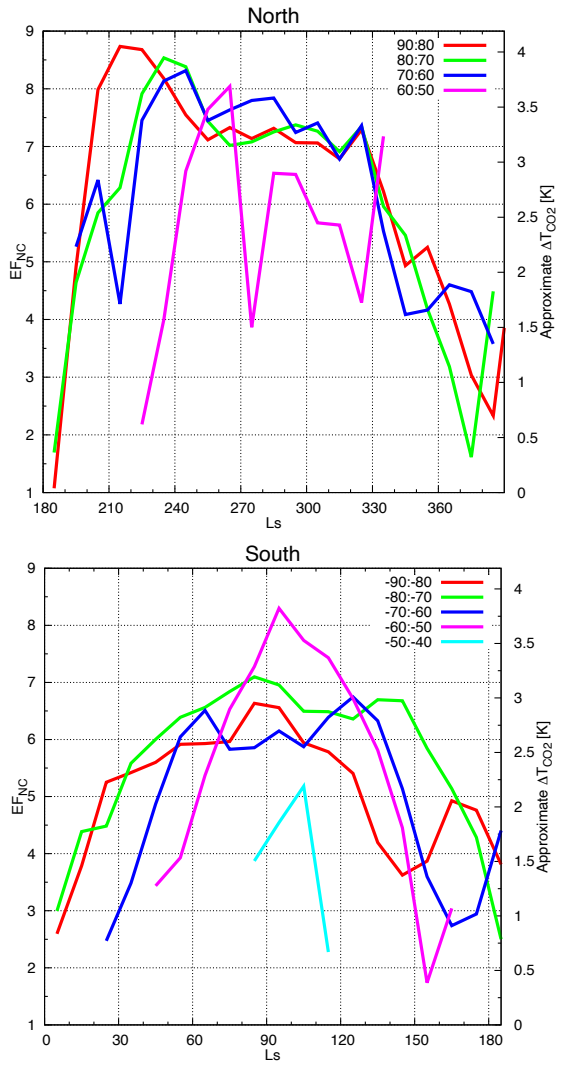

Figure 3: *Non-condensable gases enrichment (EF_{NC}, Eq. 1-3) for the North and South polar regions (10° latitudinal resolution, see key in the upper right of each panel) as a function of season. Error bars are not shown for clarity, but are typically +/- 0.13 K (med.) or +/- 0.45 K (avg.), corresponding to EF_{NC} +/- 0.26 (med.) or +/- 0.85 (avg).*

face enrichment of any latitudinal bin during most of the fall and winter, maybe as a result of the annular structure of the north polar vortex modeled by [34].

In the South, MCS data unveil a more latitudinally homogeneous enhancement peaking at EF_{NC} ~ 6-7 with the notable exception of the 40°-50°S band that only displays limited depletion (Fig. 4), and the 60-50°S band that stands out with a significantly more depleted near-surface atmosphere than the other latitudinal bands (EF_{NC} ~ 8). The dates of peak depletions are not well defined and are somewhat variable with latitude: between 80° < L_s < 100° for 90-80°S, near Ls ~ 80° for 80-70°S, and around Ls ~ 110° for 70-60°S. A lesser peak followed by a CO_2 enrichment is also observed near 60° < Ls < 70°, and near Ls ~ 100° for latitude 60-50°S. These also generally correspond to the time when the surface condensation rate is reaching its maximum. Unlike in the North, no seasonal EF_{NC} oscillations are noted at lower latitudes, although in mid/late-winter (130° < Ls < 160°), the northernmost latitudes seem to experience a complex phase of CO_2 injection and depletion. When the cap has reached its maximum mass near Ls ~ 170° [31], the enhancement process has probably shut down and atmospheric mixing (meridional and vertical) has returned the near-surface to a quasi-non-depleted state.

We interpret the remarkably homogeneous EF_{NC} values in the North and South along a wide range of latitudes as the result of efficient meridional mixing preventing the formation of measurable gradients inside the vortex, maybe helped by density-driven winds [35], despite the latitudinal dependence of surface condensation/sublimation rates [31].

The approach described in this abstract requires CO_2 ice to be present on the ground. The Gamma Ray Spectrometer [32], in contrast, generates data on non-condensable enhancement all year round and characterizes the entire atmospheric column. Our approach consisting of deriving the CO_2 partial pressure from the surface temperature only informs the state of the surface/atmosphere interface, and does not bear any information on vertical trends within the air column. In the South, the similar EF_{NC} at the surface and over the entire column indicates efficient vertical mixing and does not suggest layering of the atmosphere. But for the North where the surface depletion is significantly higher at the ground compared to the column-integrated value, we use a simple two-layer atmosphere model where the bottom layer is set to EF_{NC} = 8 as determined in this work, and an upper undepleted layer where EF_{NC} = 1 (consistent with [36]) to determine the approximate thickness h of the near-surface depleted layer. We assume an atmosphere in hydrostatic equilibrium.

A column-integrated depletion consistent with GRS data, i.e., 1 < EF_{NC} < 2 requires the near-surface depleted layer < 1 km in height (*Fig. 4*) to satisfy both the MCS and GRS observations. When considering the reported GRS uncertainties (i.e., +/- 0.5 in EF_{NC}), the depleted layer could also be strictly confined to the very surface if the column-integrated depletion is EF_{NC} ~ 1, or reach up to ~ 2 km if the column-integrated depletion is EF_{NC} ~ 2 (Fig. 5). If the depleted near-surface layer were to be thicker, the column-integrated EF_{NC} would need to be larger than reported in the literature [12,14]. The more pronounced near-surface inversions in the North compared to the South as mentioned above and reported by [37] and others might explain the differential constriction of vertical diffusion or circulation close to the surface in the North compared to South. This difference in behavior at the poles may correspond to another expression of the North versus South Hadley circulation strength, or vortex permeability driven by orbital [38] and topographic [39] asymmetries in global circulation.

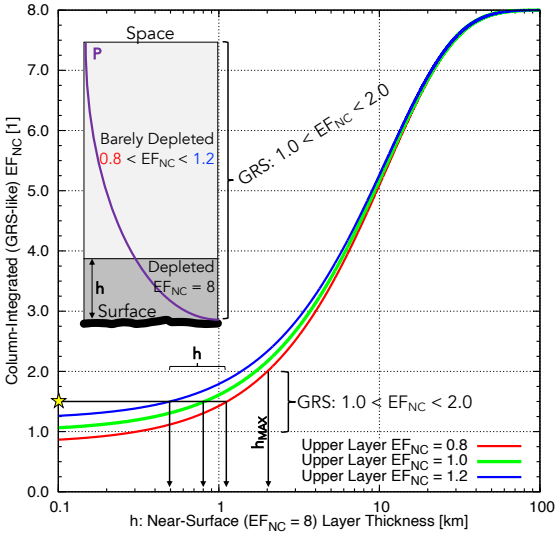

Figure 4: *Two-layer atmosphere model of a column-integrated equivalent non-condensable enhancement factor EF_{NC} (Y-axis) vs. depleted surface layer thickness (h, X axis). GRS data indicate a peak column-integrated EF_{NC} ~1.5 +/- 0.5 in the North (yellow star, [12]) derived near Ls ~ 270°. Such low column-integrated depletion requires a near-surface depleted layer (EF_{NC} ~ 8, this study) in the order of ~1-2 km in height. The upper layer is considered undepleted with EF_{NC} = 1 [36]. Top Left: schematics of the simple 1D two-layer atmospheric model used to constrain the thickness of the surface depleted layer. Purple curve illustrates the hydrostatic pressure assumption with a scale height of 11 km.*

Conclusions: MCS measures radiances consistent with wintertime CO_2 depletion of the near-surface atmosphere in both hemispheres. The distinct spatial and seasonal enhancement patterns illustrate the complex interplay between surface condensation/sublimation, fresh air injection into the polar vortices, snowfall formation and atmospheric supersaturation, as well as other fundamental differences between the North and South in the fall and winter. In the South, the depletion trend is consistent with little net transport out of the polar vortex relative to the condensation mechanism generating depletion, and the magnitude of this depletion (EF_{NC} ~ 6-7 at peak, up to ~ 8 in the 60-50°S band) in both GRS and GCM data suggests that the very near surface air has similar compositional properties as the bulk of the atmospheric column. In contrast, in the North, the near-surface depletion is significantly larger than derived from GRS data or GCM results (EF_{NC} up to 8.7 vs. 1-2). In this case, the atmospheric column is not well mixed, despite the high buoyancy of the depleted gas and a simple two-layer model indicates that the near-surface depleted layer cannot exceed ~ 2 km in height. The process preventing efficient vertical mixing with the atmosphere at higher altitudes is not identified, but we note that radio science retrievals have flagged subtle temperature inversions in the North. GCM runs also suggest inefficient vertical transport during the Northern winter. Generally, large temporal EF_{NC} oscillations unique to the 50-60° band in the North could be linked to the expression of turbulent eddies injecting non-depleted air in the vortex, and as such, this works highlights how surface temperature can be used to constrain atmospheric dynamics and benchmark modeling tools. In both hemispheres, the surface radiation is lowered by ~0-10% as a function of season and latitude due to the 0-4 K depression of the frost point, impacting CO_2 ice formation, but not dominant in the energy balance compared to other known processes.

Acknowledgements: Part of this work was performed at the Jet Propulsion Laboratory, California Institute of Technology, under a contract with NASA. This work is funded by MRO/MCS.

References: [1] R. B. Leighton and B. C. Murray, Science **153**, 136 (1966). [2] Kieffer *et al.*, Science **194**, 1346 (1976). [3] P. O. Hayne *et al.*, Journal of Geophysical Research-Planets **117**, E08014 (2012). [4] H. H. Kieffer *et al.*, Journal of Geophysical Research **82**, 4249 (1977). [5] C. W. Snyder, Journal of Geophysical Research **84**, 8487 (1979). [6] F. Forget and J. Pollack, Journal of Geophysical Research **101**, 16 (1996). [7] P. O. Hayne *et al.*, Icarus **231**, 122 (2014). [8] F. Forget *et al.*, Journal of Geophysical Research **100**, 21 (1995). [9] F. Forget *et al.*, Icarus **131**, 302 (1998). [10] R. Ditteon and H. H. Kieffer, Journal of Geophysical Research **84**, 8294 (1979). [11] C. Cornwall and T. N. Titus, Journal of Geophysical Research **114**, 11 (2009). [12] A. L. Sprague *et al.*, Journal of Geophysical Research-Planets **117**, E04005 (2012). [13] A. L. Sprague *et al.*, Science **306**, 1364 (2004). [14] A. L. Sprague *et al.*, Journal of Geophysical Research **112** (2007). [15] F. Forget, Science **306**, 1298 (2004). [16] D. J. McCleese *et al.*, Journal of Geophysical Research **112** (2007). [17] P. B. James *et al.*, in *Mars*, edited by H. H. Kieffer *et al.* (Univ. of Arizona Press, Tucson, 1992), pp. 934. [18] S. J. Greybush *et al.*, Geosci. Data J. **6**, 137, e7733 (2019). [19] M. I. Richardson *et al.*, Journal of Geophysical Research-Planets **112**, 29, E09001 (2007). [20] M. T. Zuber *et al.*, Journal of Geophysical Research **97**, 7781 (1992). [21] S. Piqueux *et al.*, Icarus **251**, 164 (2015). [22] G. B. Hansen, Journal of Geophysical Research **102**, 21569 (1997). [23] G. B. Hansen, Journal of Geophysical Research **104**, 16471 (1999). [24] G. B. Hansen, Icarus **225**, 869 (2013). [25] H. H. Kieffer *et al.*, Journal of Geophysical Research **105**, 9653 (2000). [26] C. E. Gary-Bicas *et al.*, Journal of Geophysical Research-Planets **125**, 20, e2019JE006150 (2020). [27] D. A. Paige, California Institute of Technology, 1985. [28] H. H. Kieffer *et al.*, Icarus **16**, 47 (1972). [29] H. B. Franz *et al.*, Planetary and Space Science **109**, 154 (2015). [30] W. V. Boynton *et al.*, Journal of Geophysical Research **97**, 7681 (1992). [31] M. L. Litvak *et al.*, Advances in Space Research **36**, 2156 (2005). [32] D. P. Mulholland *et al.*, Icarus **264**, 465 (2016). [33] S. R. Lewis *et al.*, Icarus **264**, 456 (2016). [34] W. J. M. Seviour *et al.*, Journal of the Atmospheric Sciences **74**, 1533 (2017). [35] S. L. Hess, Journal of Geophysical Research **84**, 2969 (1979). [36] Y. Lian *et al.*, Icarus **218**, 1043 (2012). [37] R. Y. Hu *et al.*, Journal of Geophysical Research-Planets **117**, E07002 (2012). [38] M. I. Richardson and R. J. Wilson, Nature **416**, 298 (2002). [39] A. M. Zalucha *et al.*, Journal of the Atmospheric Sciences **67**, 673 (2010).